Imaging of Acoustic Phonon Stop Bands in Superlattices

D. C. Hurley, S. Tamura,[a] and J. P. Wolfe
Department of Physics and Materials Research Laboratory, University of Illinois at Urbana-Champaign, Urbana, Illinois 61801
and
H. Morkoc
Coordinated Science Laboratory, University of Illinois at Urbana-Champaign, Urbana, Illinois 61801
(Received 9 February 1987)

Phonon-imaging experiments reveal the angular distribution of high-frequency acoustic-phonon transmission through an $In_{0.15}Ga_{0.85}As/AlAs$ superlattice. Phonon stop bands due to Bragg reflection at the folded-zone boundary are observed for both longitudinal and fast transverse phonons. A newly predicted intrazone stop band due to coupling between acoustic modes is detected.

PACS numbers: 63.20.Dj, 62.65.+k, 68.35.Gy, 68.65.+g

The layering of two alternating materials to create a superlattice imposes on the system a periodicity different from that of the crystalline lattice. Electrons and phonons with wavelengths equal to twice the superlattice period undergo Bragg reflection, leading to a rich variety of phenomena. In this paper we examine the effect of superlattice periodicity on high-frequency acoustic-phonon propagation. Using the phonon-imaging technique, we observe gaps in the phonon transmission spectrum—phonon stop bands—which depend on the phonon polarization and propagation direction. Comparison of experimental images to theoretical transmission rates not only reveals the existence of Bragg reflections at the boundary of the folded Brillouin zone, but also indicates a new type of stop band interior to the zone. The new stop band involves coupling between the longitudinal and transverse modes at oblique incident angles, and can be explained by a generalized form of the Bragg scattering condition.

Bragg reflection of short-wavelength phonons by superlattices were demonstrated experimentally by Narayanamurti *et al.* in GaAlAs/GaAs superlattices[1] and observed more recently by Koblinger *et al.* in SiO_2/Si amorphous superlattices.[2] These experiments employed phonon-spectroscopy techniques, i.e., varying of the phonon frequency and monitoring of the *time-integrated* intensity of phonons at *normal* incidence to the interfaces. In both cases, dips in the transmission were observed that matched the standard Bragg reflection condition[3] $n\lambda = 2D$, where λ is the phonon wavelength, $D = d_1 + d_2$ is the superlattice period for layer thicknesses d_1 and d_2, and n is an integer.

The basic question we address is how phonons with arbitrary propagation directions interact with a superlattice. For a phonon of wave vector $\mathbf{k}$, simple Bragg reflection dictates $n\lambda = 2D\cos\theta_k$, where $\cos\theta_k = \hat{\mathbf{k}}\cdot\hat{\mathbf{z}}$ and $\hat{\mathbf{z}}$ is a unit vector normal to the superlattice interface. Equivalently, the Bragg condition is $k_\perp = \pi n/D$, where $k_\perp = \mathbf{k}\cdot\hat{\mathbf{z}}$ is the component of the phonon wave vector normal to the interface. Phonon propagation through a superlattice is especially interesting because (1) as a result of the anisotropy the energy flux (or group velocity) is in general not parallel to $\mathbf{k}$, and (2) three modes of propagation—one longitudinal and two transverse—are involved in the reflection process at an interface. The first factor gives rise to bulk "phonon focusing," whereby the heat flux emanating from a point source is highly anisotropic. The second factor allows the possibility of coupling between the modes and mode conversion at an interface—effects which are not present in the cases of electromagnetic-wave or electronic propagation through periodic structures.

Figure 1 shows the calculated dispersion relation ν vs $k_\perp$ for acoustic phonon propagation through an InGaAs/AlAs superlattice at a particular angle of incidence. Longitudinal (L), fast transverse (FT), and slow transverse (ST) branches are shown. Band gaps (phonon stop bands) appear at the zone center and folded-zone boundary with bandwidths Δ_L, Δ_{FT}, and Δ_{ST}. In addition, as predicted recently,[4] a coupled-mode stop band of width $\Delta_{L\text{-}ST}$ appears interior to the zone and is due to coupling between L and ST vibrations which are mixed together by mode conversion at the superlattice interfaces. [For propagation in the (100) plane, no mixing occurs between L and FT or ST and FT phonons.] Physically, the coupled-mode stop band may be viewed as an intermode Bragg reflection with the conditions $k_\perp^L + k_\perp^{ST} = 2\pi n/D$, $\omega_L = \omega_{ST}$, and $k_\parallel^L = k_\parallel^{ST}$, where $k_\perp^{L,ST}$ are positive normal components. It should be noted that as the angle of incidence θ_k increases, the branches on the ν versus $k_\perp$ diagram become steeper and thus the frequencies of the stop bands increase, as predicted by the Bragg condition. Hence, in a fixed-frequency experiment, one or more stop bands may be detected by scanning of the propagation angle.

Phonon imaging provides a measure of the phonon transmission through a crystal as a continuous function of propagation angle.[5] The present experiments require selection of phonon frequency and velocity (or mode) in addition to requiring high spatial resolution. A focused

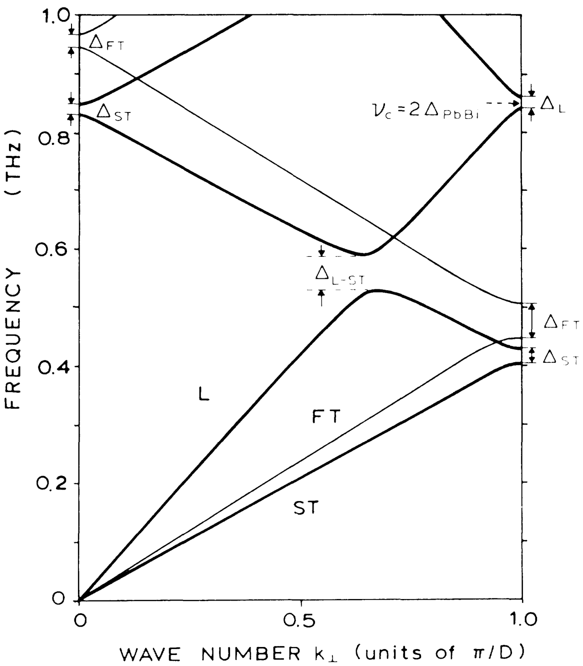

FIG. 1. Acoustic-phonon dispersion relation $\nu=\nu(k_\perp)$ for a (001)-$In_{0.15}Ga_{0.85}As/AlAs$ superlattice, where $k_\perp$ is the normal component of the phonon wave vector. The angle of incidence in the GaAs substrate is $\theta_k=32.5°$ in the (100) plane for L phonons. [The corresponding real-space direction is indicated by point A in Fig. 2(d).] The conservation of $k_\parallel$ implies $\theta_k=20°$ and 18° for FT and ST phonons, respectively. The folded-zone boundary is at $k_\perp=\pi/D$, with $d_1=d_2=D/2=20$ Å. Phonon stop bands occur at the folded-zone center and boundary (widths Δ_L, Δ_{FT}, and Δ_{ST}), as well as inside the zone (width $\Delta_{L\text{-}ST}$). The cuton frequency ν_c of the PbBi detector is also indicated.

laser beam (cavity-dumped Ar^+ pulses, $\lambda=5145$ Å, width=15 ns, energy=0.1 μJ) is raster scanned across the (100) surface of an undoped GaAs substrate (~400-μm-thick wafer) immersed in liquid helium ($T\approx1.8$ K). The excitation surface is covered with a 2000-Å Cu film to localize the heat source. Phonons created by the thermal relaxation of photoexcited Cu electrons propagate ballistically across the substrate and through a superlattice grown by molecular-beam epitaxy (MBE) on the other side. The superlattice consists of 40 periods of $In_{0.15}Ga_{0.85}As/AlAs$, with single-layer thickness $d_1=d_2=20$ Å. The phonons are detected by a 20×20-μm^2 PbBi superconducting tunnel junction evaporated directly onto the superlattice. The tunnel junction has a sharp sensitivity cuton at a frequency ν_c corresponding to twice the superconducting gap. The gap size is controlled by adjusting the relative amount of Bi used in the evaporation, permitting a cut-on range $650\le\nu_c\le850$ GHz which can be measured from the junction's I-V characteristics. The junction's tunneling current (proportional to the phonon flux) is the input signal to a boxcar averager which selects the different phonon polarization modes (L and T) by their differing times of flight (boxcar gate width ~35 ns). The output signal is digitized for each position of the laser beam and displayed as a relative intensity on a video monitor, creating a two-dimensional map of phonon intensity versus phonon propagation direction.

The phonon image for L phonons in such a system $\nu_c=850$ GHz) is shown in Fig. 2(a). To produce this image, the boxcar delay time was continuously adjusted to be proportional to the ballistic path length at each laser position, thus selecting a constant velocity. This affords almost total separation between the L and T modes. The most obvious feature in Fig. 2(a) is the dark ring corresponding to a narrow dip in intensity centered on the (100) direction. This slightly anisotropic ring occurs at angles $\theta_V\approx35°-37°$ from the axis, which is close to that predicted for the first-order zone-boundary stop band, labeled Δ_L in Fig. 1. Specifically, $\theta_V=39°$ ($\theta_k=32.5°$) was chosen in Fig. 1 in order to match the Δ_L stop band exactly with $\nu_c=850$ GHz.[6] A 2-Å uncertainty in the layer thickness, or the use of nondispersive elastic theory, could account for the small discrepancy between theory and experiment.

The sharpness of the transmission dip in the experimental image indicates that a relatively narrow frequency range is sampled by the detector. The width of the dip, $\Delta\theta_V\approx7°$, implies $\Delta_\nu\approx150$ GHz. This suggests that the GaAs substrate—an undoped commercial wafer—must be limiting the transmission of ballistic phonons with $\nu\gtrsim1$ THz. A high-frequency cutoff of this sort can be caused by mass-defect scattering from naturally occurring isotopes[7] or residual impurities.[8] In the present case, such frequency-selective scattering ($1/\tau\sim\nu^4$ for isotopes) is a highly desirable factor which, in conjunction with the sharp high-pass sensitivity of the tunneling junction, produces a quasimonochromatic selection of phonons.

To isolate better the effect of the superlattice, we etched the superlattice off the substrate and repeated the experiment. As expected, without the superlattice the dark ring is absent, as shown in Fig. 2(b). The difference between images with and without the superlattice is shown in Fig. 2(c) with increased gain. The dark regions signify phonons that were not transmitted through the superlattice. The difference image also brings out another striking effect of the superlattice which was not so prominent in the original image, namely the anisotropic diamond-shaped feature surrounding the $n=1$ ring. This reduction in transmitted flux is *not* due to a higher-order reflection. (For $n\ge2$, $\cos\theta_k>1$ under these conditions.)

To gain a quantitative understanding of these results, we have performed a calculation of the stop-band distribution for this system, Fig. 2(d), assuming a band of frequencies 850–900 GHz. The narrow circular stop-band ring agrees well with that in the experimental image. The theory also shows the diamond-shaped feature

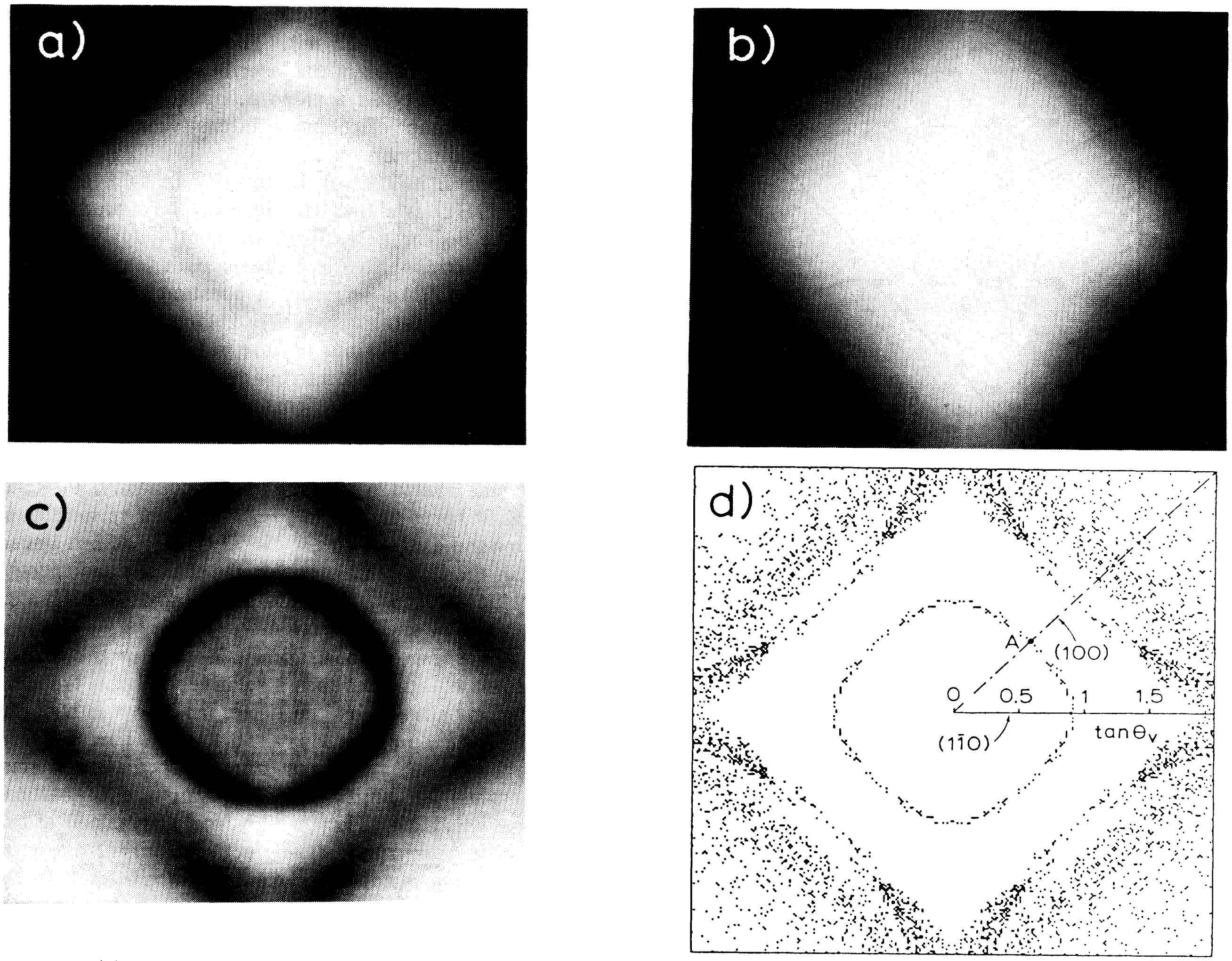

FIG. 2. (a) Image of longitudinal phonons ($v = 5.35$ km/s) transmitted through a GaAs substrate and an $In_{0.15}Ga_{0.85}As$/ AlAs superlattice. Detector cuton frequency is $\nu_c = 850$ GHz. The dark ring is due to Bragg-reflected phonons when $\cos\theta_k = \lambda/2D$. The image represents a scan of approximately $\pm 60°$ from left to right, with the (100) direction at the center of the image. (b) Corresponding image for GaAs substrate only. (c) Differential phonon image in which dark regions represent a reduction in phonon transmission by the superlattice. Obtained by subtracting (b) from (a), adding an offset, and increasing the gain. To improve the signal-to-noise ratio, the four symmetry-related quadrants have been added together. (d) Calculated angular distribution of L-phonon stop bands for the same case. Full crystalline anisotropy is included, as described in Ref. 3. The polar angle is denoted by θ_V.

present in the experimental image. This feature is due to coupled-mode stop bands ($\Delta_{\text{L-ST}}$) within the zone. In Fig. 2(d), the relatively denser regions near {110} planes are due to L-FT coupling; the remainder near {100} planes are primarily due to L-ST coupling. The noncircular shape of the diamond structure arises mainly from the anisotropy of the T modes.

Tracking a slower velocity allows detection of the transverse modes, as indicated in Fig. 3. In this experiment, the detector cut-on frequency is $\nu_c = 700$ GHz. Bright features are due to phonon focusing in the GaAs crystal. Close inspection of the region indicated by arrows reveals an interesting effect due to the superlattice. Both a dip in the transmission and a slight shift in the positions of the FT phonon-focusing caustics are apparent in this image. A theoretical calculation of the phonon stop band helps to explain these effects. Figure 4(a) shows the predicted FT stop bands for a frequency of 700 GHz, the lowest frequency present in the experimental phonon image. For 900-GHz phonons, the FT zone-boundary stop band (Δ_{FT}) shifts further away from ⟨100⟩, as indicated in Fig. 4(b). However, the FT caustic for 700- and 900-GHz phonons are separated as a result of dispersion,[7,9] as shown in Fig. 4(c). Combining these effects, we show schematically in Fig. 4(d) the expected intensity pattern for a *distribution* of frequencies between 700 and 900 GHz. All phonons in this frequency range display a small common gap of reduced

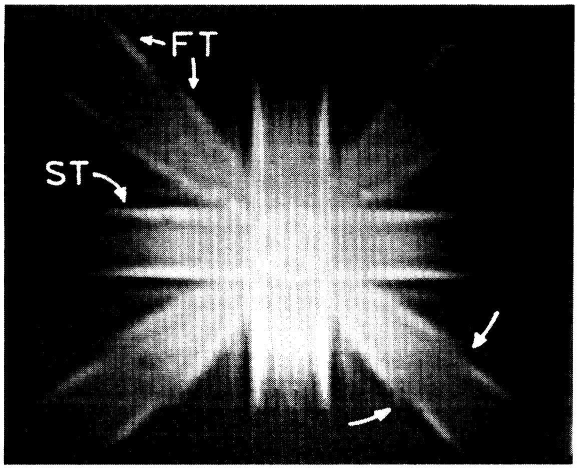

FIG. 3. Constant-velocity ($v = 3.35$ km/s) phonon image of transverse phonons (FT and ST) in $In_{0.15}Ga_{0.85}As/AlAs$ superlattice, $\nu_c = 700$ GHz. The image scale and orientation are approximately the same as in Fig. 2. A 25-μm Gaussian broadening due to finite laser spot and detector resolution has been deconvolved from this image. The arrows indicate a Bragg scattering due to the superlattice.

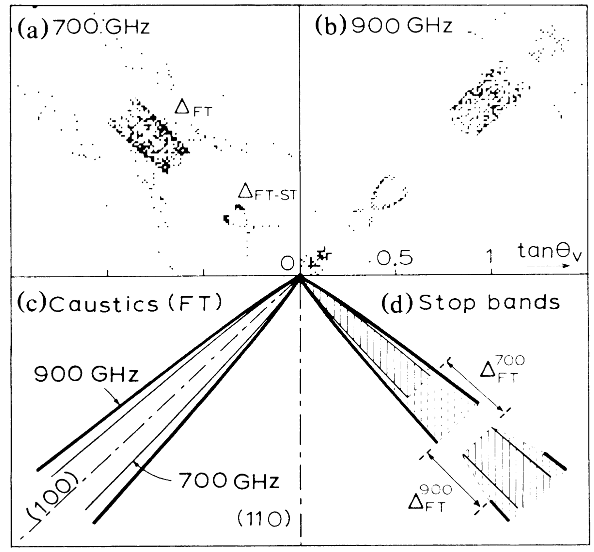

FIG. 4. Theoretical calculations for the case in Fig. 3. (a),(b) the stop-band distributions for 700- and 900-GHz phonons from the theory of Ref. 3 are depicted, respectively. (c) Schematic of the FT caustics formed at 700 and 900 GHZ. Dispersion in the bulk GaAs causes the shift in their positions. (d) Schematic representation of the phonon stop-band effect for a range of frequencies 700–900 GHz.

transmission. This gap and the apparent shifting of the caustics are precisely what is observed in the experimental image of Fig. 3.

These initial experiments reveal an interesting variety of new phenomena associated with high-frequency acoustic phonon transmission through a superlattice. Phonon detection with small, high-quality PbBi superconducting tunnel junctions yields the simultaneous resolution of phonon propagation angle, frequency, and velocity (or mode) necessary to observe the angular distribution of superlattice stop bands. The highly anisotropic nature of this problem involves a combination of classical phonon topics—phonon dispersion, mode conversion, and evanescent wave formation—which can be readily studied by imaging techniques.

We would like to thank J. Worlock for stimulating discussions on this topic. We are grateful to J. Chen and T. Henderson for help with sample preparation. Support for this work was provided by U.S. National Science Foundation Grant No. DMR-83-16981 (experiments and calculations) and by U.S. Department of Energy Grant No. MRL-DE-AC02-76ER01198 (MBE sample preparation). Equipment support was also provided by U.S. National Science Foundation Grant No. 85-21444. One of us (S.T.) acknowledges a travel grant by the Department of Education, Science, and Culture of Japan.

[a]Permanent address: Department of Engineering Science, Hokkaido University, Sapporo 060, Japan.

[1]V. Narayanamurti, H. L. Störmer, M. A. Chin, A. C. Gossard, and W. Wiegmann, Phys. Rev. Lett. **43**, 2012 (1979).

[2]O. Koblinger, J. Mebert, E. Dittrich, S. Döttinger, and W. Eisenmenger, in *Phonon Scattering in Condensed Matter V*, edited by A. C. Anderson and J. P. Wolfe (Springer-Verlag, New York, 1986), p. 156.

[3]S. M. Rytov, Akust. Zh. **2**, 71 (1956) [Sov. Phys. Acoust. **2**, 68 (1956)].

[4]S. Tamura and J. P. Wolfe, Phys. Rev. B **35**, 2528 (1987).

[5]For a recent review of the phonon-imaging technique, see G. A. Northrop and J. P. Wolfe, in *Nonequilibrium Phonon Dynamics*, edited by W. E. Bron (Plenum, New York, 1985), Chap. 5.

[6]In numerical calculations, the following values were used: For AlAs, $\rho = 3.76$ g/cm^3, $C_{11} = 120.2$, $C_{12} = 57.0$, and $C_{44} = 58.9$ (units of 10^{10} dyn/cm^2); for $In_{0.15}Ga_{0.85}As$, $\rho = 5.41$ g/cm^3, $C_{11} = 114.0$, $C_{12} = 53.0$, and $C_{44} = 56.4$ (units of 10^{10} dyn/cm^2). [See S. Adachi, J. Appl. Phys. **58**, R3 (1985); R. Reifenberger, M. J. Keck, and J. Trivisonno, J. Appl. **40**, 5403 (1969).]

[7]W. Dietsche, G. A. Northrop, and J. P. Wolfe, Phys. Rev. Lett. **47**, 660 (1981); G. A. Northrop, S. E. Hebboul, and J. P. Wolfe, Phys. Rev. Lett. **55**, 95 (1985); S. E. Hebboul and J. P. Wolfe, Phys. Rev. B **34**, 3948 (1986).

[8]V. Narayanamurti, M. A. Chin, and R. A. Logan, Appl. Phys. Lett. **33**, 481 (1978).

[9]S. Tamura, Phys. Rev. B **25**, 1415 (1982), and **28**, 897 (1983).

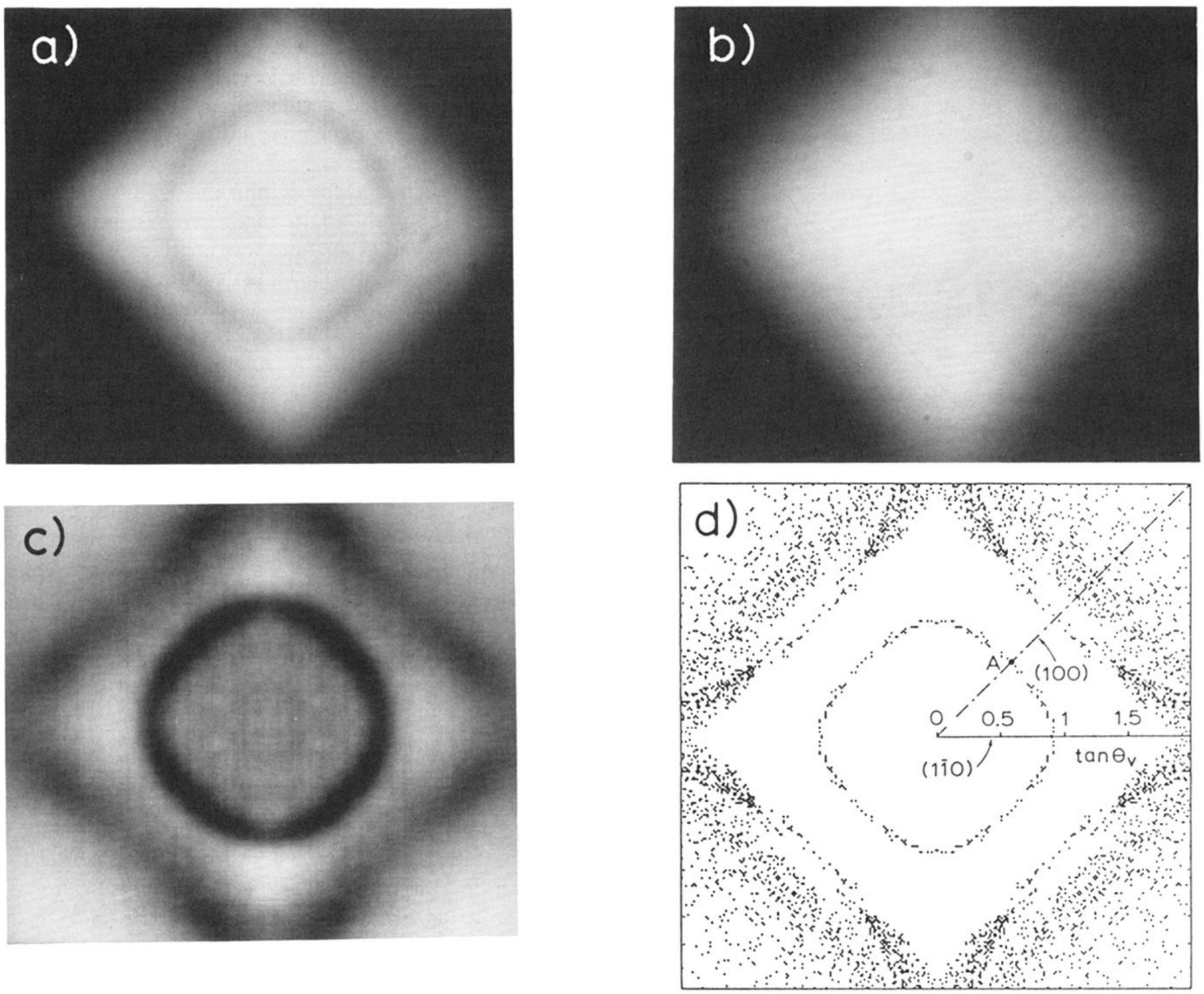

FIG. 2. (a) Image of longitudinal phonons ($v = 5.35$ km/s) transmitted through a GaAs substrate and an $In_{0.15}Ga_{0.85}As$/ AlAs superlattice. Detector cuton frequency is $\nu_c = 850$ GHz. The dark ring is due to Bragg-reflected phonons when $\cos\theta_k = \lambda/2D$. The image represents a scan of approximately $\pm 60°$ from left to right, with the (100) direction at the center of the image. (b) Corresponding image for GaAs substrate only. (c) Differential phonon image in which dark regions represent a reduction in phonon transmission by the superlattice. Obtained by subtracting (b) from (a), adding an offset, and increasing the gain. To improve the signal-to-noise ratio, the four symmetry-related quadrants have been added together. (d) Calculated angular distribution of L-phonon stop bands for the same case. Full crystalline anisotropy is included, as described in Ref. 3. The polar angle is denoted by θ_V.

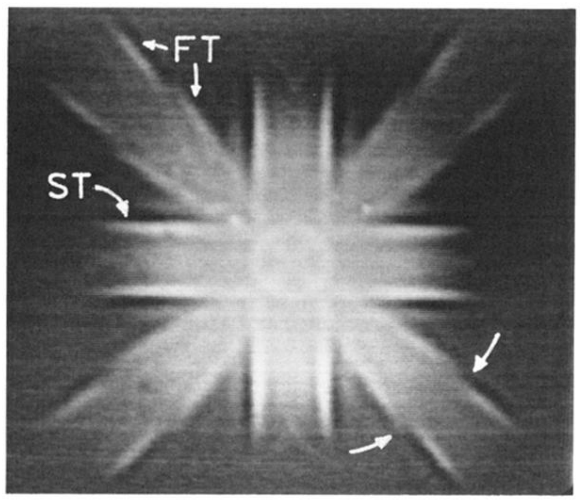

FIG. 3. Constant-velocity ($v=3.35$ km/s) phonon image of transverse phonons (FT and ST) in $In_{0.15}Ga_{0.85}As/AlAs$ superlattice, $\nu_c=700$ GHz. The image scale and orientation are approximately the same as in Fig. 2. A 25-μm Gaussian broadening due to finite laser spot and detector resolution has been deconvolved from this image. The arrows indicate a Bragg scattering due to the superlattice.